Propagation of a chemical wave front in a quasi-two-dimensional superdiffusive flow

A. von Kameke,* F. Huhn, G. Fernández-García, A. P. Muñuzuri, and V. Pérez-Muñuzuri
Group of Nonlinear Physics, University of Santiago de Compostela, E-15782 Santiago de Compostela, Spain
(Received 6 April 2010; published 18 June 2010)

Pattern formation in reaction-diffusion systems is an important self-organizing mechanism in nature. Dynamics of systems with normal diffusion do not always reflect the processes that take place in real systems when diffusion is enhanced by a fluid flow. In such reaction-diffusion-advection systems diffusion might be anomalous for certain time and length scales. We experimentally study the propagation of a chemical wave occurring in a Belousov-Zhabotinsky reaction subjected to a quasi-two-dimensional chaotic flow created by the Faraday experiment. We present a novel analysis technique for the local expansion of the active wave front and find evidence of its superdiffusivity. In agreement with these findings the variance $\sigma^2(t) \propto t^\gamma$ of the reactive wave grows supralinear in time with an exponent $\gamma > 2$. We study the characteristics of the underlying flow with microparticles. By statistical analysis of particle trajectories we derive flight time and jump length distributions and find evidence that tracer-particles undergo complex trajectories related to Lévy statistics. The propagation of active and passive media in the flow is compared.

DOI: 10.1103/PhysRevE.81.066211 PACS number(s): 89.75.Kd, 47.27.De, 47.54.De, 82.40.Ck

I. INTRODUCTION

The propagation of passive and active tracers in chaotic flows is a field of study of enormous interest for a variety of different disciplines reaching from biology over chemistry and physics as far as financial mathematics and social studies [1–4]. Especially the influence of advection on the spatiotemporal development of active media is of relevance for many natural systems such as plankton species in the ocean, atmospheric chemistry or convection in the earth mantle [5]. For these reaction-diffusion-advection systems it is of crucial interest to define typical dynamics as pattern formation or the speed of propagation. An experimentally and theoretically well studied active system, producing spatiotemporal patterns and reaction fronts, is the Belousov-Zhabotinsky reaction (BZ) [6] that we use in this study. For the induction of a fluid flow we use the Faraday experiment, which consists in the vertical vibration of the fluid. This vibration excites surface waves and bulk fluxes [7–9].

Reaction fronts of target waves in reaction-diffusion systems travel with a constant velocity v_{front} that is usually obtained from the Fisher-Kolmogorov-Petrovskii-Piskunov (FKPP) prediction,

$$v_{front} = 2\sqrt{Dk}, \tag{1}$$

where D is the molecular diffusion constant and k is the reaction rate [6,10,11]. Reaction-diffusion-advection systems are often described by replacing the molecular diffusion constant D with an effective diffusion constant D^*. However, recent experiments have shown that the FKPP prediction does not hold for the case of enhanced diffusion caused by a fluid flow that induces chaotic mixing [11]. Additionally, normal enhanced diffusion might not be a good approximation for some important time and length scales of a chaotic flow. In this case the assumption that the underlying random walk of the reactants can be described by a probability function with a finite second moment (i.e., Gaussian distribution) does not hold. This raises the question how dynamics change when the system exhibits superdiffusion.

Superdiffusion is defined as the supralinear growth of the variance $\sigma^2(t)$ of the probability density function (PDF) $P(\vec{r},t)$

$$\sigma^2(t) \propto t^\gamma, \quad \text{with} \quad \gamma > 1. \tag{2}$$

The PDF gives the probability to find a particle at position $\vec{r}$ at time t. In one dimension the variance $\sigma^2(t)$ can be written as

$$\sigma^2(t) = \int_{-\infty}^{\infty} (x - \langle x \rangle)^2 P(x,t) dx, \tag{3}$$

where $\langle x \rangle$ is the expectation value of the PDF.

Superdiffusive behavior of tracers can arise due to a variety of different processes. In real flows, superdiffusion is an effect created by the imperfection of the turbulence, i.e., the existence of coherent structures in the velocity field [12,13]. The microscopic theory underlying this general random walk is called continuous time random walk (CTRW) and was formulated by Montroll and Weiss [14] and extended to the multistage random walk theory (MSRW) by Shlesinger and Klafter [15]. This probabilistic point of view is especially useful in systems where the full information about the underlying velocity field and its evolution in time is not known, as it is the case in our experiments. Passive particles that experience superdiffusive transport for certain time and length scales in chaotic flows have been studied experimentally [16–21] and numerically [22–26] by a variety of different groups. Even though numerical and theoretical studies of reaction-superdiffusion systems exist, they focus (to our knowledge) on one dimensional systems and can be divided into two different classes of which the first deals with bistable reaction processes [27–29] while the second class deals with oscillatory or excitable reaction dynamics [30]. Experimental studies of active media in this context are more scarce [7,11,31–33]. The difficulties of studying active media

*Corresponding author; alejandra@fmares.usc.es

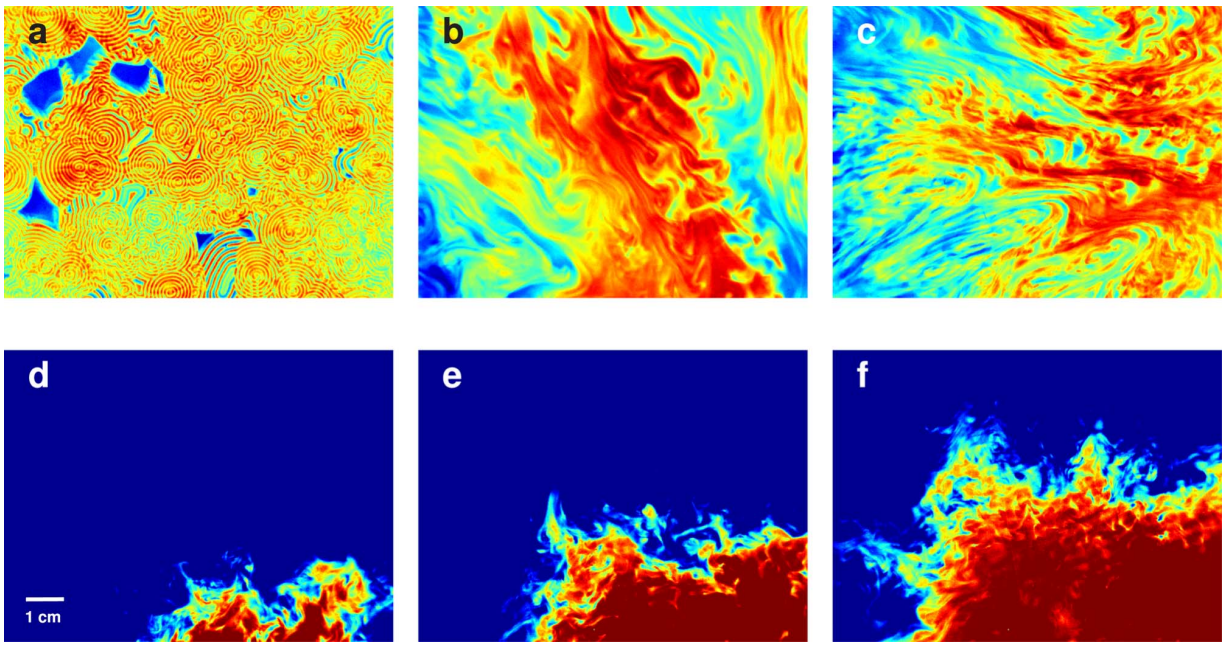

FIG. 1. (Color online) Patterns observed for the BZ reaction subjected to different frequencies and accelerations of vertical vibration (Faraday Experiment). Transitional changes in the patterns are observed and different regions of pattern formation can be distinguished as the forcing increases. (a) Without forcing the typical targets and spirals of the BZ reaction are observed [6]. (b) and (c) For a forcing of $f=20$ Hz and $f=30$ Hz ($a=1\ g_0$) filamentary patterns develop. (d)-(f) For a forcing of $f=60$ Hz and $a=0.5\ g_0$ a single advection phase wave propagates through the reactor.

experimentally with a probabilistic approach arise from the dilemma that the underlying statistics are only valid for point particles in the flow while active media is studied in terms of concentration fields. Expressions for the PDFs [or equally: concentrations $c(\vec{r},t)$] that solve the master equations in the continuum limit (CL) depend strongly on the specific underlying microscopic random walk process [4,34] and do not have a simple closed formulation. A consequence of this dilemma is the intricacy of finding measureable variables (other than the variance growth of the concentration-field) that can be compared to the existing theory.

Figure 1 shows different patterns we have observed in a Belousov-Zhabotinsky reaction exposed to a horizontal flow produced by the Faraday experiment [8,9]. The most striking pattern observed is an activator wave that periodically propagates through the entire reactor [Figs. 1(d)–1(f)]. We will focus on this activator wave and will refer to it as advection phase wave [33]. In this paper, we propose a novel approach for the analysis of the propagation of a chemical wave in a superdiffusive flow that is based on the simple assumption that in a first approximation small volumes of the activator experience random displacements just as particles would. In Sec. II, a description of the experimental setup and procedure for the measurements with active and passive media in the flow is given. Section III describes the statistical analysis techniques used and puts special emphasis on the theory of the underlying stochastical processes. In Sec. IV, the results are presented. We show that the flow is superdiffusive and that particles in the flow experience Lévy walks which results in superdiffusion and an anomalous variance growth $\sigma^2(t)=t^\gamma$, with $\gamma>1$. We find that the reactive front on the time and length scales measured also propagates superdiffusively and that the velocity of the front propagation is not constant. Finally, in Sec. V, we compare and discuss the results from active and passive media experiments.

II. EXPERIMENTAL PROCEDURE

A. Setup

Figure 2 shows a schematic of the experimental setup. The experiments are conducted in a circular reactor of 30 cm diameter with an inner border that reduces capillary effects [35] (Inset Fig. 2). A large diameter of the reactor is chosen to reduce boundary effects in the center of the reactor where measurements are performed. The reactor is fixed on top of an electromagnetic shaker (TIRAvib S511, TIRA GmbH) that produces vertical vibration. The acceleration of the reactor is modulated as $g(t)=g_0+a\cos(wt)$, where g_0 is the gravitational acceleration. The shaker supplies a 75 N rated peak force, a maximum acceleration of 50 g_0, a maximum rated travel of 10 mm and a clean frequency range of 2 Hz to 7000 Hz, as specified by the manufacturer. It is connected to a power amplifier which receives a sinus signal from a function generator (HP 33120A). The acceleration and the frequency of forcing of the reactor are measured by a piezoelectric accelerometer (PCB piezotronics M353B18) and a power signal conditioner (PZB piezotronics 480C02) and finally read out by an oscilloscope (HP 54645). The reactor where the chemicals are deposited is made of transparent plexiglass and illuminated from below by a custom made backlight. The selected field of view is 8.0×10.7 cm^2 and is kept constant throughout all experiments. Images are recorded with a monochrome firewire camera (Guppy, AVT) at a frame rate

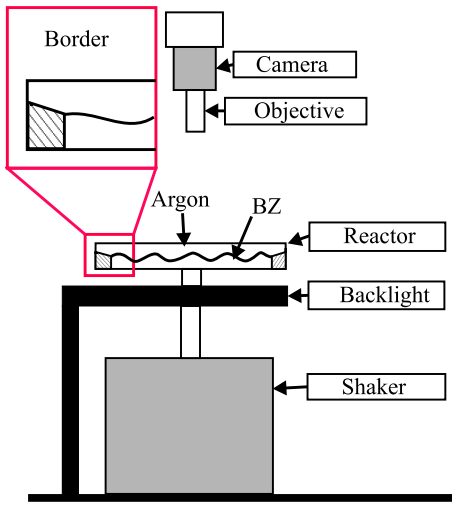

FIG. 2. (Color online) Schematic diagram of the experimental setup. A circular reactor made of plexiglass is filled with liquid (BZ or water) up to a height of 2 mm. The reactor is fixed on top of an electromagnetic shaker and vertical vibrations produced by the shaker induce Faraday waves and fluxes in the liquid. To minimize influence of capillary effects on the creation of Faraday waves the reactor is constructed with an inner border that closes up with the liquid surface [35]. BZ experiments are conducted under an inert atmosphere of argon. Experiments are illuminated with a backlight and monitored with a camera.

of 60 Hz and a resolution of 480×640 pixel^2, so that 1 pixel$\approx$0.017 cm. For further processing images are stored to a hard disk and analyzed off-line as described in Sec. III.

The Faraday waves obtained in the experiments have all rectangular or hexagonal shape for the forcing range studied and a fluid layer of 2 mm. The wavelength is 0.5 cm–1.0 cm and the dominant wave frequency is half the forcing frequency (subharmonic response) [8,36]. For all forcings applied the wave pattern observed is time-dependent, i.e., for the lower forcings defects in the Faraday wave pattern travel through the reactor and for higher forcings the defects dominate the pattern.

It is known that Faraday patterns exhibit well-defined order-disorder transition for increasing forcing frequency and amplitude, leading from standing waves to a disordered state where the translational correlation length drops dramatically and the orientational correlations of the patterns also decreases [36]. This disorder in the patterns is sometimes referred to as spatiotemporal chaos [37]. Thus the higher the forcing strength and the frequency the more rapid are the fluctuations of the observed patterns. The fluctuation or defects in the ordered wave patterns are due to a transverse amplitude modulational instability.

Fluid flows induced by this wave patterns are termed spatiotemporally chaotic, an intermediate case between low-dimensional chaotic systems and fully developed turbulence [16]. Particles on the surface of these flows can undergo very complex trajectories and the properties of the transport can be described by statistical means [16,18,19]. Additionally, in a thin fluid layer such as in the experiment (2 mm), convective fluxes are induced that may enhance the long range displacement of particles in the flow [38].

B. Experiments with chemical reaction

The recipe for the aqueous solution of the BZ reaction was chosen in order to obtain a high contrast for recording. The exact concentrations are: cyclohexandion 1 M, sulfuric acid 6 M, sodium bromate 1 M and ferroin 0.025 M. With these concentrations the BZ reaction is in the oscillatory regime as was measured by means of spectroscopy. The reactants are mixed in strictly the same order for each experiment and stirred for 60 min. Then the reactants are poured into the reactor on top of the shaker. The reactor is filled up to a height of 2 mm and inert argon gas is injected for 15 min to avoid oxygen inhibition in the BZ dynamics [39,40]. The recipient is then closed with a transparent plexiglass cover and the BZ reaction is left to rest for another 15–20 min until the typical patterns of an BZ reaction, targets and spirals, occur [Fig. 1(a)]. Then the forcing is slowly switched on and another 15 min are given to the system to become resonant before recording is started. During the recording the strength of the forcing is continuously monitored with an accelerometer. Experiments are performed for a frequency range of 10–70 Hz (in steps of 10 Hz) and accelerations a of 0.5 g_0, 0.75 g_0, 1 g_0, and 1.5 g_0. The upper limit of the forcing range is given by the onset of droplet formation on the surface of the liquid and wetting of the cover which makes recording unfeasible. The room temperature was kept constant at 23 ± 1 °C during all experiments.

C. Experiments with particles

For the experiments with particles pure water is chosen as fluid media because it gives a better contrast for image analysis than the BZ solution and has very similar properties concerning density, viscosity and surface tension. The particles (Black CromoSpheres, Brookhaven Instruments) have a mean diameter of 502 ± 24 μm with a density of $d\approx1.06$ g/cm^3 slightly higher than the density of water at room temperature (23 °C, 1.00 g/cm^3). Despite that higher density particles usually float on the surface of the fluid and only a few particles sink and are thus sorted out. For the experiment with the particles the same reactor as for the chemical experiments is used, changing only the transparent cover with a nearly identical one that has a hole of the diameter 0.5 cm to facilitate the application of the particles. Particles are applied to the reactor one after the other and the trajectories are recorded until the particles leave the field of view. Experiments are performed for a frequency range of 30–60 Hz (in steps of 10 Hz) and an acceleration of $a=1$ g_0. In order to ensure the validity of the free particle approximation, the Stokes number S that quantifies the Stokes drag needs to be small, $S\ll1$ [21]. It can be calculated as $S\approx Ud^2/18\nu L$ where U is a typical velocity of the particles, d is their diameter, ν is the viscosity and L is a typical length scale of the flow. In our experiments the Stokes number S is of the order 10^{-2} so the particles behave sufficiently passive.

III. ANALYSIS

The analysis is split into two parts. The first introduces analysis concepts used for the passive particles in the flow

and the second part focuses on the description of the analysis technique applied to the advection phase wave in the BZ reaction. The analysis of the advection phase wave is based on the assumption that some characteristics of the particle motion also represent the movement of finite fluid volumes.

A. Analysis of the random walks of the particles

The chaotic dynamics of a particle in a fluid flow is an intermediate case in between completely random (nonintegrable) and completely regular (integrable) kinetics. CTRW is an important model for the description of this chaotic dynamics and can be applied to experimental measurements of particle trajectories (for a discussion of different models see [41]).

1. Concepts of continuous time random walk theory

We want to summarize some of the important concepts of CTRW theory following the arguments presented elsewhere [15,34,42,43]. In CTRW theory the trajectory of a particle in a fluid flow is described statistically by three elementary functions, the jump length distribution $p(\Delta R)$, the waiting time distribution $\varphi(\Delta t_{wait})$ and the flight time distribution $q(\Delta t_{flight})$. A walker (a particle) is assumed to make a jump of length ΔR and duration Δt_{flight} to a resting point where it rests a time Δt_{wait} until the next jump. From these three distributions the expression for the probability density function $P(\vec{r},t)$ to find a particle at time t at the point $\vec{r}$ can be derived [15]. Thus, also the evolution of the variance $\sigma^2(t)$ [Eq. (3)] can be written in terms of these three distributions [41,44,45]. In a real turbulent flow the particle is never at rest and the waiting time can be neglected. Hence, $P(\vec{r},t)$ is calculated using only the jump length and the flight time distribution and, importantly, some assumption about the coupling of the jump length and flight time which introduces the concept of Lévy walks [15,44,46]. Lévy walks arise when the jump length and the flight time distribution are coupled such that longer jumps take longer times to complete due to a finite velocity of the particles in real flows. The coupled probability of a jump to last a time Δt_{flight} and overcome thereby a distance ΔR can be written as [15]

$$\Phi(\Delta R,\Delta t_{flight}) = p(\Delta R|\Delta t)q(\Delta t_{flight}) \tag{4}$$

or equivalent

$$\Phi(\Delta R,\Delta t_{flight}) = q(\Delta t_{flight}|\Delta R)p(\Delta R), \tag{5}$$

where we consider that ΔR is the jump distance $|\vec{r}|$ and the process is isotropic. The probabilities in Eqs. (4) and (5) obey the experimentally useful relationships [15]

$$\sum_{\Delta R} \Phi(\Delta R,\Delta t_{flight}) = q(\Delta t_{flight}) \tag{6}$$

and

$$\sum_{\Delta t} \Phi(\Delta R,\Delta t_{flight}) = p(\Delta R). \tag{7}$$

These independent probability distributions on the right hand side of Eqs. (6) and (7) can be measured experimentally by defining the turning points of the trajectory of the random walker. The distance between these turning points is defined as the jump length ΔR and the duration of the jump as the flight time Δt. Superdiffusion ($\sigma^2(t) \propto t^\gamma, \gamma > 1$) occurs when the flight time and the jump length distributions have heavy tails of the form

$$q(\Delta t_{flight}) \propto \Delta t^{-\eta} \tag{8}$$

$$p(\Delta R) \propto \Delta R^{-\mu_p}. \tag{9}$$

In order to obtain the variance growth from Eqs. (8) and (9), two different coupling laws have been studied theoretically by different authors [15,44,45,47]. The first coupling model, for turbulent flows, was suggested by Shlesinger and Klafter [15]

$$q(\Delta t_{flight}|\Delta R) = \delta\left(\Delta t - \frac{|\Delta R|}{|V(\Delta R)|}\right), \tag{10}$$

where δ denotes the δ-function and $V(\Delta R)$ is an expression for turbulent velocity. They show that if this coupling is considered for the calculation of $P(\vec{r},t)$ it leads to an exponent γ_{turb} of the variance growth [Eq. (3)],

$$\gamma_{turb} = \begin{cases} 3 & \text{if } (\mu_p - 1) \le \frac{1}{3} \\ 2 + \frac{3}{2}(2 - \mu_p) & \text{if } \frac{1}{3} \le (\mu_p - 1) \le \frac{5}{3} \\ 1 & \text{if } (\mu_p - 1) \ge \frac{5}{3} \end{cases}. \tag{11}$$

The second frequently discussed coupling is of the form

$$q(\Delta t_{flight}|\Delta R) = \delta(\Delta t^\nu - \Delta R), \tag{12}$$

where the temporal and the spatial step are coupled by a δ function. For a given time step Δt the points that can be reached with one spatial step lie on a shell around the starting point and the exponent ν which can be calculated from μ_p and η defines the scaling between the time and the spatial steps. This coupling leads to a different expression for the variance growth exponent, here denoted as γ_ν that is more complicated and thus not shown here (for a detailed description see [44,45]). These two different couplings will be used for an estimation of the variance growth exponent γ from the measurements of exponents μ_p and η.

2. Definition of experimental random walk process

The particle position data $\vec{r}(t)$ obtained from our experiments has a temporal resolution of 60 Hz and a subpixel spatial resolution. In order to obtain the jump length distribution $p(\Delta R)$ and the flight time distribution $q(\Delta t)$ the turning points of the random walk in radial direction have to be defined. Figure 3 shows a random walk derived by this definition. As the isotropy of the flow is indispensable for this definition, the congruence of the jump distributions in x- and y-direction of the image coordinates has been verified. An arbitrary starting point $\vec{r}(t_0)$ from the position data is selected as the first turning point. The point $\vec{r}(t_n)$ where the radial distance

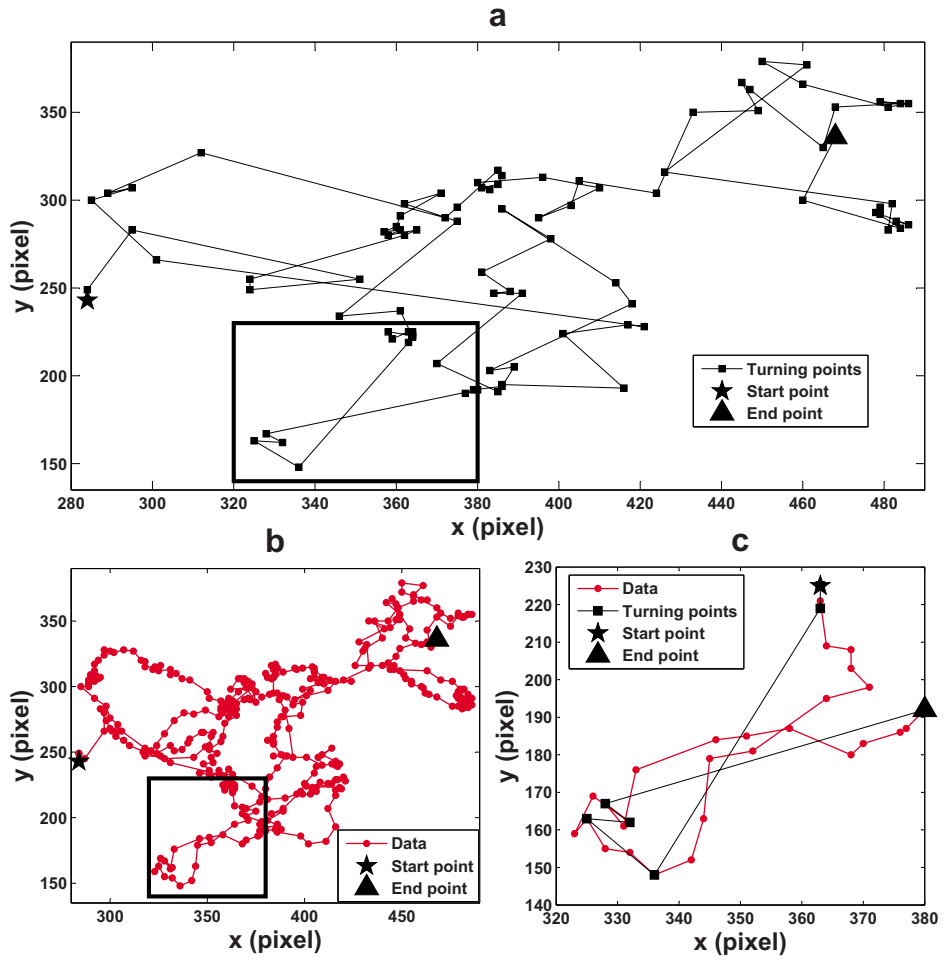

FIG. 3. (Color online) a) A typical random walk trajectory (forcing: 60 Hz, $a=1\ g_0$) where the turning points (black squares) are obtained from recorded data points shown in b). The random walk shows a variety of different scales of the jump length ΔR. The lack of a typical length scale leads to heavy-tailed jump length distributions that cause superdiffusion. b) The original measured data of the trajectory (red dots). Note the small high frequency oscillations of the particle due to the Faraday waves. This oscillations do not contribute to the overall displacement of the particle. c) Detail from the highlighted frame in a) and b) presented in order to illustrate the definition of the turning points (data: red dots, turning points: black squares). Whenever the distances between the current turning point $\vec{r}(t_0)$ and two following data points $\vec{r}(t_{n+1})$ and $\vec{r}(t_n)$ behaves as $\Delta R_{n+1} < \Delta R_n$ the data point $\vec{r}(t_n)$ is chosen as a new turning point and the same procedure is applied to it. In this way successively a set of turning points is obtained (see also Sec. III A 2). The high oscillations due to the Faraday waves are mostly filtered out by this procedure.

$$\Delta R_n = |\vec{r}(t_0) - \vec{r}(t_n)| \tag{13}$$

reaches its first maximum is set as the next turning point and the new starting point for the algorithm.

We obtain the jump length distributions Eq. (6) and flight time distributions Eq. (7) from the random walk and estimate the heavy-tail exponents μ_p and η Eqs. (8) and (9) by fitting (see Fig. 4). The exponents μ_p and η together with a theoretical assumption of the coupling law for Δt and ΔR as introduced in Eqs. (10) and (11) determine the exponent γ of the variance growth. In Sec. IV A, the variance growth exponents γ_ν and γ_{turb} will be calculated from μ_p and η and compared to the directly measured values of the variance growth.

B. Analysis of the wave front

Figure 1 shows the different regimes observed in the BZ patterns in dependence of the forcing acceleration and frequency and the resulting flow. Without forcing, the typical target and spiral patterns of the BZ reaction can be seen [Fig. 1(a)]. Above a critical forcing the patterns observed exhibit important structural changes. For weak forcing (forcing acceleration and forcing frequency low, e.g., $f=20$ Hz, $a=0.75\ g_0$), targets and spirals are only slightly stretched (not shown). Then, for a higher forcing filamentary patterns appear [Figs. 1(b) and 1(c), e.g., $f=20$ Hz, $a=1\ g_0$]. For an even stronger forcing multiple advection phase waves appear in different parts of the reactor (not shown) and finally, if the forcing is further augmented, a single advection phase wave propagates from one side of the reactor to the other [Fig. 1(d)–1(f), e.g., $f=60$ Hz, $a=0.5\ g_0$]. When the forcing is too strong, all patterns disappear and the media becomes totally homogeneous [7] (see Fig. 7 for an overview of the parameter range where advection phase waves are observed). This is remarkable, especially because after switching off the forcing the typical spirals and targets reappear again. This

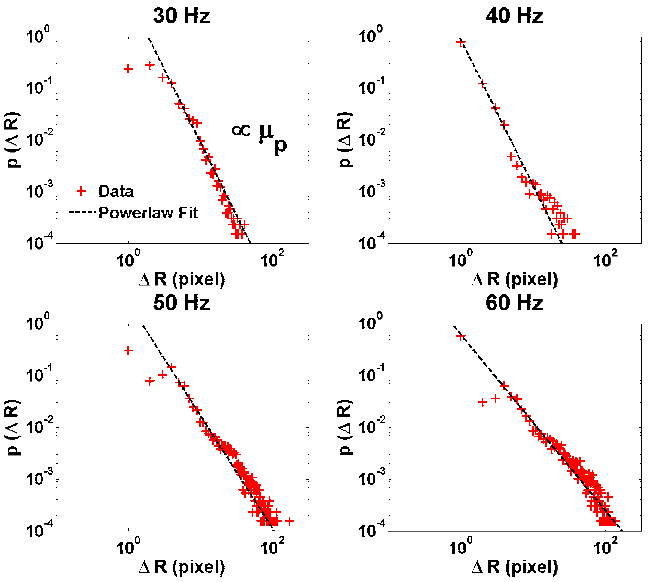

FIG. 4. (Color online) Jump length distributions of the particle experiments $p(\Delta R)$ [Eq. (9)] for the different forcing frequencies derived from the data (log-log scale). The exponents μ_p (2.8 ± 0.1, 2.6 ± 0.1, 2.2 ± 0.1, 1.7 ± 0.1) are obtained by fitting a power law (dashed line) to the jump length distributions for the different forcing frequencies (30 Hz, 40 Hz, 50 Hz, 60 Hz, and $a=1\ g_0$).

circumstance itself already suggests that the advection phase wave is not a mere effect of enhanced mixing but critically depends on the detailed dynamics of the flow. The absence of any pattern above a critical forcing seems to coincide with droplet formation on the surface of the liquid and thus with an instability of the Faraday waves.

The direct way to characterize the front dynamics of the advection phase wave is the measurement of the variance growth of the activator spot in time. Exemplary measurements of the variance growth have been realized. The variance was calculated from the images as the weighted sum of the squared radii of the area covered by the advection phase wave at time t: $\sigma_r^2(t)=\Sigma_r r^2 w_r(t)$, where $w_r(t)$ is the number of occurrence of radius r. However, the initiation of an advection phase wave in the middle of the field of view by chance is a rare event as it normally starts at the boundary of the reactor, presumably due to perturbations. Provoked initiation of an advection phase wave within the field of view by introduction of a silver wire [48] proved to be difficult.

We therefore designed an analysis for the front propagation in analogy to the jump length distribution in the particle random walk described above. We define a probability $\lambda(\Delta R,\Delta t)$ to find a volume of high activator concentration after a time Δt at a distance ΔR to a beforehand defined front. This analysis is realized by an algorithm that detects the front line of an advection phase wave in an image I_t and then draws n new equidistant lines (masks) where mask_n is n pixels apart from the front line and $n\in(1,2,3,\ldots,N)$. Once these N masks are created, the intersection of image $I_{t+\Delta t}$ with each mask of the image I_t is calculated. This counts how many pixels at a distance n away from the front have become activated after a time Δt. This procedure is applied on each image pair I_t and $I_{t+\Delta t}$ while the advection phase wave passes through the field of view (around 400–500 images) and the jump distribution $\lambda(\Delta R,\Delta t)$ for jumps ahead of the front is obtained. Fitting a Lévy function [49,50] to the data allows for the extraction of an exponent μ_r that describes the heavy tail behavior of the distribution $\lambda(\Delta R,\Delta t)\propto\Delta R^{-\mu_r(\Delta t)}$. For a random walk in one (two) dimension $\mu_r<3$ (<4) implies that the walker experiences large displacements that lead to Levy walks and superdiffusion.

IV. RESULTS

This section is divided in two parts. First, the results for the particle experiments are presented and it is shown that the flow produced by the Faraday experiment is superdiffusive for forcing frequencies $f\geq40$ Hz, while at 30 Hz the flow is not superdiffusive. In the second part we show that the front of the advection phase wave also propagates superdiffusively and accelerated.

A. Particles

Figure 4 shows the jump length distributions $p(\Delta R)$ obtained for different forcing frequencies (at $a=1\ g_0$). Jump length exponents μ_p are estimated by power-law fitting to the recorded data. The flight time distribution exponents ν are obtained in the very same way from the corresponding distributions (not shown). In Table I, the exponents of the jump length and the flight time distributions are summarized. Using CTRW theory the exponents γ_ν and γ_{turb} for the variance growth are calculated from μ_p and ν as described in Sec. I and shown in Table I. For the values of the exponents μ_p and ν extracted from these fittings CTRW theory predicts super-

TABLE I. List of exponents μ_p (jump length distribution) and η (flight time distribution) [Eqs. (8) and (9)] for the particle random walks (at $a=1\ g_0$). From these values we calculate the theoretically derived variance growth exponents (γ_ν, γ_{turb}) and compare it to the measured ones γ_{exp}. At higher frequencies the theoretical values exceed the measured ones and overestimate the superdiffusivity considerably.

		30 Hz	40 Hz	50 Hz	60 Hz
Experiment	μ_p	2.8 ± 0.1	2.6 ± 0.1	2.2 ± 0.1	1.7 ± 0.1
	η	1.9 ± 0.2	2.3 ± 0.2	1.9 ± 0.2	1.8 ± 0.2
	γ_{exp}	1.0 ± 0.1	1.3 ± 0.1	1.4 ± 0.1	1.3 ± 0.1
From theory	γ_ν	≈1.4	≈1.5	≈1.7	≈2.1
	γ_{turb}	≈1	≈1.1	≈1.7	≈2.45

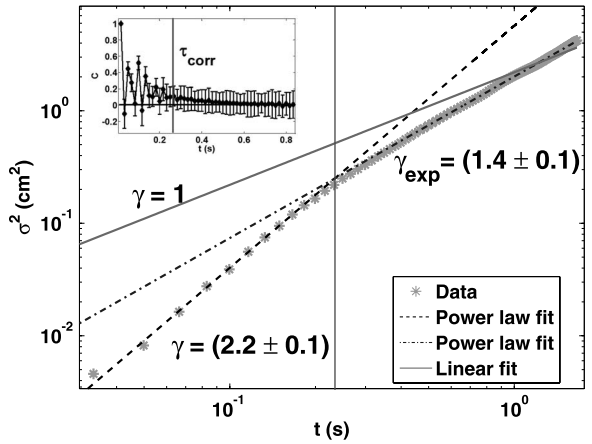

FIG. 5. Variance growth of the particle experiments (50 Hz, $a=1\ g_0$, log-log scale). Two different regimes can be identified: Up to a correlation time τ_{corr} the variance growth is close to ballistic (dashed line) while above that time the variance grows superdiffusively (dash-dotted line) with an exponent $\gamma_{exp}=1.4\pm0.1$. For comparison a power-law with an exponent $\gamma=1$ as expected for normal diffusion is plotted (continuous line). Inset: The correlation time (vertical bar) can also be estimated from the velocity autocorrelation function.

diffusion, $\gamma>1$, except for γ_{turb}(30 Hz). This indicates the lack of a typical scale in the dynamics of the flow, even though there is a largest scale as the experimental setup has finite boundaries.

Figure 5 shows the measured variance growth directly obtained from particle trajectories. The experimental variance growth exponents γ_{exp} are extracted by power-law fits to the data. The directly measured variance growth for a forcing of $f=50$ Hz at $a=1\ g_0$ is shown for time scales of considerable importance for the dynamics compared to velocity values in the range of some cm/s. The variance is calculated from 200 different experiments. Clearly a transition from a ballistic growth of the variance $\gamma\approx2$ to a superdiffusive $1<\gamma_{exp}<2$ can be observed in the data and is accounted for by two different fitting regimes.

The experimentally obtained values of γ_{exp} for the different forcing frequencies are also found in Table I to facilitate comparison to the derived values γ_ν and γ_{turb}. The inset in Fig. 5 shows the velocity autocorrelation function $C=\vec{v}_{t+\Delta t}\vec{v}_t/(|\vec{v}_{t+\Delta t}||\vec{v}_t|)$. This function sheds light on the time scales τ_{corr} on which the flow is still correlated. The ballistic growth of the variance changes to superdiffusive around that correlation time τ_{corr}.

Comparing the different variance growth exponents γ in Table I, we find a transition from normal diffusion to superdiffusion in the flow in between 30–40 Hz (at $a=1\ g_0$) for γ_{exp} and γ_{turb}. The values of exponent γ_ν do not show this transition. In contrast to the derived γ_ν and γ_{turb} the directly obtained γ_{exp} does not show a strong increase toward higher values of the forcing frequency. This suggests that the real coupling in between Δt and ΔR in the flow differs from the two theoretical ones and that they overestimate the superdiffusion.

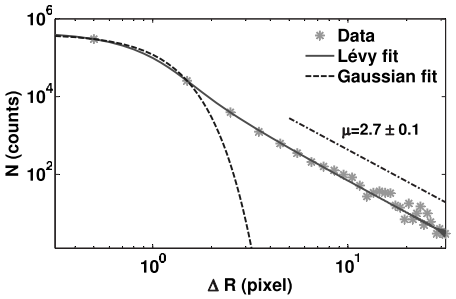

FIG. 6. The probability distribution $\lambda(\Delta R,\Delta t)$ for activator volumes to jump a distance ΔR perpendicular to the reaction front is well fitted by a Lévy function (continuous line). A Gaussian distribution (dashed line) underestimates the probability of large displacements. The dash dotted line shows the heavy tail behavior of the Lévy fit from which the exponent $\mu_r=2.7\pm0.1$ is obtained. An exponent $\mu_r<3$ expresses that the activator volumes experience Lévy walks which can lead to superdiffusion. Data (50 Hz, $a=1\ g_0$, $\Delta t=1/60$ s) are shown on log-log scales and obtained from around 550 image pairs using the masking algorithm described in Sec. III B.

B. Active media

The superdiffusion in the flow is also observable in the dynamics of the advection phase wave. Figure 6 shows that the jump length distribution of the front $\lambda(\Delta R,\Delta t)$ is well described by a Lévy function while a Gaussian strongly underestimates the probability for long jumps of activator volume. An exponent α is obtained from the Lévy fit [49,50], where $\mu_r=\alpha+1$ is the behavior of the heavy tail of $\lambda(\Delta R,\Delta t)$. An exponent $\mu_r(\Delta t)<3$ signifies that on local time and length scales the front propagates superdiffusively and the volumes of high activator concentration exhibit Lévy walks.

Figure 7 shows the exponents $\mu_r(\Delta t)$ as a function of the frequency and the amplitude of the forcing for two different Δt ($\Delta t=1/60$ s and $\Delta t=2/60$ s). We find that the exponent $\mu_r(\Delta t)$ decreases with increasing forcing, i.e., long jumps get more probable. Also long jumps are slightly more probable for larger times Δt [Fig. 7(b)]. Figure 7 also visualizes the limited parameter range for which an advection phase wave exists. The white fields represent forcing parameters where no clear single advection phase wave could be observed.

Figure 8 shows the variance growth $\sigma_r^2(t)\propto t_r^\gamma$ of a centered advection phase wave in time. We find that for an experiment with a forcing frequency of $f=50$ Hz at $a=1\ g_0$ the variance of the advection phase wave monitored grows with an exponent $\gamma_r=3.4\pm0.2$ and that the mean displacement in radial direction $\langle r(t)\rangle$ grows with $\zeta=1.7\pm0.2$ (data not shown). For other forcing strengths and triggered advection phase waves, values of γ_r lie in the same range.

We conclude that $\gamma_r>2$ and $\zeta>1$ which indicates that the front of the advection phase wave travels in an accelerated way and not with a constant velocity. Qualitative observations suggest that intervals of propagation with constant velocity interchange with intervals of constant acceleration when parts of the front move rapidly forward with jets occurring in the flow.

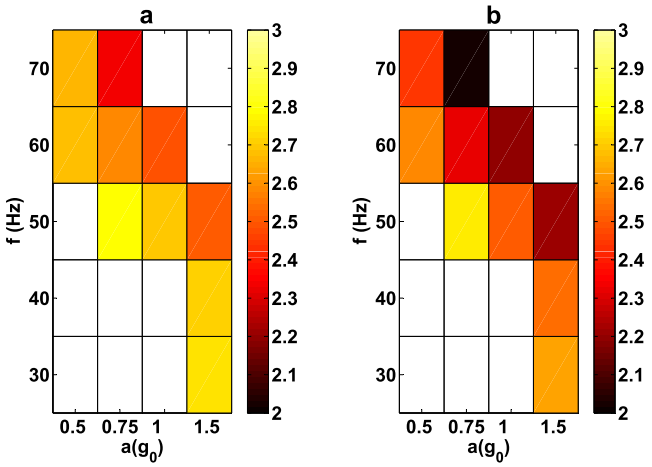

FIG. 7. (Color online) Heavy-tail exponent $\mu_r(\Delta t)$ obtained from jump length distribution of the reaction front. The exponent decreases for higher forcing (in frequency and in amplitude) and longer times (a) $\Delta t=1/60$ s, b) $\Delta t=2/60$ s) which indicates that the probability to make a long jump increases. For all advection phase waves analyzed the exponent is in the range $2<\mu_r(\Delta t)<3$ and thus superdiffusive propagation of the front is expected. A single advection phase wave that propagates through the whole reactor can only be observed for a confined range of the forcing parameters (colored fields).

V. DISCUSSION

The quasi-two-dimensional flow produced by the Faraday experiment experiences a transition from normal diffusion to superdiffusion around a forcing frequency of 30–40 Hz ($a=1\ g_0$). This has been shown by analyzing the trajectories of micro-particles applied to the flow at different forcing frequencies. Two different analysis techniques were used:

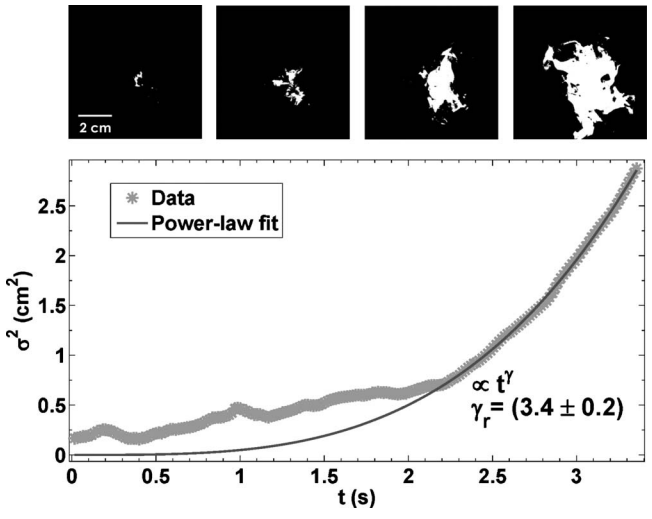

FIG. 8. Variance growth of a centered reactive wave (asterisks)(50 Hz, $a=1\ g_0$). A power-law $\sigma_r^2(t)\propto t^{\gamma_r}$ with $\gamma_r=3.4\pm0.2$ fits the data after a continuous spot has formed (continuous line). This indicates that the front of the advection phase wave propagates in an accelerated way in the superdiffusive flow. Top: Binary image series shows the expansion of the active spot ($\Delta t\approx0.84$ s in between frames).

application of concepts from CTRW theory and direct measurement of the variance growth.

The BZ reaction subjected to the Faraday experiment exhibits important structural changes in dependency of the forcing parameters. For a limited parameter range a single advection phase wave can be observed that propagates from one side of the reactor to the other. The propagation of the wave front is analyzed with the described masking algorithm. Probability distributions for jumps of activator volumes perpendicular to the reaction front are obtained for different forcings. The distributions are well fitted by Lévy functions which allows for the extraction of heavy-tail exponents $\mu_r(\Delta t)$. These exponents are a measure for the probability of long jumps. A value $\mu_r(\Delta t)<3$ indicates superdiffusion on the considered time scale. The values $\mu_r(\Delta t)$ decrease for higher forcings and longer times Δt which means that long jumps become more probable. Exemplary variance measurements for the advection phase wave show a variance growth in time that is supralinear which signifies that the wave front propagates accelerated and the front velocity increases with time.

Comparison of the results obtained from particle experiments with the results from the analysis of the advection phase wave indicates that superdiffusivity of the flow is an important requirement for the occurrence of an advection phase wave. The transition of the flow from normal diffusion to superdiffusion observed with the particles happens around the same frequency (40 Hz, $a=1\ g_0$) as the transition in the BZ reaction from filamentary patterns to advection phase wave occurrence. However, a direct quantitative comparison of the analyzed variables [as the variances γ_{exp} and γ_r or the jump length distribution exponents μ_p and $\mu_r(\Delta t)$] from the particle experiments and the advection phase wave experiments is awkward for a variety of reasons. First, the microscopic description of a random walk with reaction differs from a description of a passive random walk, because there is an additional reaction probability for the activator. To our knowledge such statistical descriptions of random walks with active media exist only for bistable reactions [27–29,51,52] and not for oscillatory or excitable media as we have studied in our experiment. Second, the suggested analysis of the reaction front using the masking algorithm is only valid for short time steps Δt when the overall shape of the front between two images has not changed much. Therefore, the exponents $\mu_r(\Delta t)$ depend on the time step and can only be reliably derived for short times Δt. In spite of this limitation, the masking algorithm can be an option for the description of the dynamics of systems where variance growth measurements are not practicable. Especially the application of the masking algorithm to the reactive waves occurring in bigger reactors or in nature might be worthwhile where it can be unfeasible to capture the whole reactive wave with a sufficient spatial resolution. In particular, when length and time scales of practical importance are small compared to the scales of the entire reactive wave, the propagation of the irregular front can be characterized by the masking algorithm. Possible applications could be waves in geophysical flows like plankton blooms in the ocean [2] or depletion of ozone layer [53], among others.

In conclusion, we have found that the quasi-two-dimensional flow in our reactor is superdiffusive for certain forcing parameters. In a BZ reaction subjected to this flow an advection phase waves occurs that propagates with accelerated front velocities. The local propagation of the wave front can be characterized by an exponent $\mu_r(\Delta t)$, which defines the probability for large jumps of activator volumes perpendicular to the reaction front.

ACKNOWLEDGMENTS

The authors thank Dr. Shock for helpful discussions and the anonymous referees for helpful comments on the manuscript. This work was financially supported by the Ministerio de Educación y Ciencia through Project No. FIS2007-64698 and by the Xunta de Galicia through Project No. PGIDIT06PXIB206169PR.

[1] R. N. Mantegna and H. E. Stanley, Nature (London) **376**, 46 (1995).
[2] M. A. Srokosz, G. D. Quartly, and J. J. H. Buck, Geophys. Res. Lett. **31**, L13301 (2004).
[3] D. Brockmann, L. Hufnagel, and T. Geisel, Nature (London) **439**, 462 (2006).
[4] R. Metzler and J. Klafter, J. Phys. A **37**, R161 (2004).
[5] Z. Neufeld and E. Hernández-García, *Chemical and Biological Processes in Fluid Flows* (Imperial College Press, London, 2010).
[6] *Chemical Waves and Patterns*, edited by R. Kapral and K. Showalter (Kluwer Academic, Dordrecht, 1993).
[7] G. Fernández-García, D. I. Roncaglia, V. Perez-Villar, A. P. Munuzuri, and V. Perez-Munuzuri, Phys. Rev. E **77**, 026204 (2008).
[8] M. Faraday, Philos. Trans. R. Soc. London **121**, 299 (1831).
[9] J. W. Miles and D. Henderson, Annu. Rev. Fluid Mech. **22**, 143 (1990).
[10] R. A. Fisher, Ann. Eugen. **7**, 355 (1937).
[11] J. R. Boehmer and T. H. Solomon, EPL **83**, 58002 (2008).
[12] M. B. Isichenko, Rev. Mod. Phys. **64**, 961 (1992).
[13] P. Castiglione, A. Mazzino, P. Muratore-Ginanneschi, and A. Vulpani, Physica D **134**, 75 (1999).
[14] E. W. Montroll and G. H. Weiss, J. Math. Phys. **6**, 167 (1965).
[15] M. F. Shlesinger and J. Klafter, J. Phys. Chem. **93**, 7023 (1989).
[16] R. Ramshankar, D. Berlin, and J. P. Gollub, Phys. Fluids A **2**, 1955 (1990).
[17] R. Ramshankar and J. P. Gollub, Phys. Fluids A **3**, 1344 (1991).
[18] E. Schröder, J. S. Andersen, M. T. Levinsen, P. Alstrom, and W. I. Goldburg, Phys. Rev. Lett. **76**, 4717 (1996).
[19] A. E. Hansen *et al.*, Phys. Rev. Lett. **79**, 1845 (1997).
[20] T. H. Solomon, E. R. Weeks, Harry L. Swinney, Phys. Rev. Lett. **71**, 3975 (1993).
[21] T. H. Solomon, E. R. Weeks, and H. L. Swinney, Physica D **76**, 70 (1994).
[22] T. H. Solomon, A. T. LEE, and M. A. Fogleman, Physica D **157**, 40 (2001).
[23] M. A. Fogleman, M. J. Fawcett, and T. H. Solomon, Phys. Rev. E **63**, 020101(R) (2001).
[24] R. Gorenflo, F. Mainardi, D. Moretti, G. Pagnini, and P. Paradisi, Physica A **305**, 106 (2002).
[25] R. N. Mantegna and H. E. Stanley, Phys. Rev. Lett. **73**, 2946 (1994).
[26] A. Blumen, G. Zumofen, and J. Klafter, Phys. Rev. A **40**, 3964 (1989).
[27] D. H. Zanette, Phys. Rev. E **55**, 6632 (1997).
[28] R. Mancinelli, D. Vergni, and A. Vulpiani, EPL **60**, 532 (2002).
[29] G. Zumofen and J. Klafter, Phys. Rev. E **50**, 5119 (1994).
[30] V. V. Gafiychuk and B. Y. Datsko, Phys. Rev. E **75**, 055201(R) (2007).
[31] M. S. Paoletti and T. H. Solomon, Phys. Rev. E **72**, 046204 (2005).
[32] M. S. Paoletti, C. R. Nugent, and T. H. Solomon, Phys. Rev. Lett. **96**, 124101 (2006).
[33] G. Fernández-García and V. Pérez-Muñuzuri, Eur. Phys. J. - Special Topics **165**, 169 (2008).
[34] R. Gorenflo and F. Mainardi, in *Anomalous Transport*, edited by R. Klages, G. Radons, and I. M. Sokolov (Wiley, Weinheim, 2008).
[35] M. T. Westra, D. J. Brinks, and W. van der Water, J. Fluid Mech. **496**, 1 (2003).
[36] N. B. Tufillaro, R. Ramshankar, and J. P. Gollub, Phys. Rev. Lett. **62**, 422 (1989).
[37] A. Kudrolli and J. P. Gollub, Physica D **97**, 133 (1996).
[38] P. H. Wright and J. R. Saylor, Rev. Sci. Instrum. **74**, 4063 (2003).
[39] O. Steinbock, C. T. Hamik, and B. Steinbock, J. Phys. Chem. A **104**, 6411 (2000).
[40] Y. Y. Kalishyn, M. Rachwaska, V. O. Khavrus, and P. E. Strizhak, Phys. Chem. Chem. Phys. **7**, 1680 (2005).
[41] G. M. Zaslavsky, Phys. Rep. **371**, 461 (2002).
[42] M. F. Schlesinger, in *Anomalous Transport*, edited by R. Klages, G. Radons, and I. M. Sokolov (Wiley, Weinheim, 2008).
[43] D. del-Castillo-Negrete, in *Anomalous Transport*, edited by R. Klages, G. Radons, and I. M. Sokolov (Wiley, Weinheim, 2008).
[44] J. P. Bouchaud and A. Georges, Phys. Rev. A **41**, 1156 (1990).
[45] X.-J. Wang, Phys. Rev. A **45**, 8407 (1992).
[46] J. Klafter, A. Blumen, and M. F. Schlesinger, Phys. Rev. A **35**, 3081 (1987).
[47] M. F. Shlesinger, B. J. West, and J. Klafter, Phys. Rev. Lett. **58**, 1100 (1987).
[48] V. Pérez-Muñuzuri, R. Aliev, B. Vasiev, V. Perez-Villar, and V. I. Krinsky, Nature (London) **353**, 740 (1991).
[49] B. J. West and W. Deering, Phys. Rep. **246**, 1 (1994).
[50] R. N. Mantegna, Phys. Rev. E **49**, 4677 (1994).
[51] D. del-Castillo-Negrete, B. A. Carreras, and V. E. Lynch, Phys. Rev. Lett. **91**, 018302 (2003).
[52] D. Brockmann and L. Hufnagel, Phys. Rev. Lett. **98**, 178301 (2007).
[53] S. Edouard, B. Legras, F. Lefevre, and R. Eymard, Nature (London) **384**, 444 (1996).